FEATURE ARTICLE

Polarization Spectroscopy of Single Fluorescent Molecules

Taekjip Ha,*,†,||,▽ Ted A. Laurence,†,‡ Daniel S. Chemla,†,‡ and Shimon Weiss*,†,§

Materials Sciences Division, Lawrence Berkeley National Laboratory, 1 Cyclotron Road, Berkeley, CA 94720, Physics Department, University of California at Berkeley, Berkeley, CA 94720, and Physical Biosciences Division, Lawrence Berkeley National Laboratory, 1 Cyclotron Road, Berkeley, CA 94720

Received: March 17, 1999; In Final Form: June 2, 1999

Polarization spectroscopy of single fluorescent molecules is used to probe their rotational dynamics. When a molecule is immobilized on a dry surface, its in-plane dipole orientation is precisely determined by utilizing its transition dipole moment. An angular offset between the absorption and the emission dipoles was detected from a single fluorophore revealing its binding geometry to the surface. In an aqueous environment, DNA-tethered fluorophores display dynamics that are well-described by a hindered rotational diffusion model. A detailed description of the model is given, including calculations to estimate depolarization effects resulting from the high numerical aperture objective used to collect fluorescence photons. Protein-conjugated fluorophores display very distinct dynamics with continuous evolution of the rotational profile, possibly reflecting fluctuations in the polypeptide chain. When protein-conjugated fluorophores are allowed to freely diffuse in solution, it is possible to determine the fluorescence polarization anisotropy of each molecule that traverses the laser beam. The anisotropy values could, in principle, be used to identify conformational states of single molecules without the potential artifacts associated with surface immobilization.

I. Introduction

Experiments that measure bulk solution properties and therefore the combined action of many molecules cannot discern distribution functions since the measured quantities will necessarily report on the average properties of the ensemble of molecules in the sample. In contrast, single-molecule studies can reveal information on the distributions of molecular properties and on the time trajectories of observables that are often hidden or distorted in conventional ensemble studies. Recent developments in room temperature detection and spectroscopy of single fluorescent molecules[1−27] are particularly promising for biological studies because they allow the observation of conformational changes of macromolecules in action. However, as has been documented extensively,[5,6,13,14,16,18,19,21,24] single fluorophores can often display various kinds of fluorescence intensity and spectral fluctuations, even in the absence of biologically relevant events. To help circumvent these issues, two properties of a single fluorescent probe attached to a macromolecule can be exploited in a way that is not possible in an ensemble study. The first is the distance dependent fluorescence energy transfer to (or from) a second fluorophore which is designed into the system. If designed properly, fluctuations in the transfer efficiency will overwhelm other sources of fluctuations. The second is its unique absorption and emission transition dipoles, which can be interrogated by polarized excitation light and/or by analyzing the emission polarization. Conformational changes can therefore be detected by measuring distance changes between two sites on the macromolecule via single-pair fluorescence resonance energy transfer (spFRET),[11,27−30] or by detecting changes in the dipole orientation of a rigidly attached probe,[13,20,25] or by their combination.

Single-molecule spectroscopy (SMS) aided by other techniques such as patch clamp, atomic force microscopy (AFM), and optical tweezers can simultaneously monitor distance/orientation changes together with mechanical or chemical activity of the macromolecule, thus correlating conformational changes with function.[23] It is hoped that these capabilities will complement traditional static structural biology tools such as X-ray crystallography and NMR by providing dynamical information on the macromolecule during reactions.[31]

The discussion in this manuscript is limited to polarization anisotropy studies of single dipoles and considers the possibility of measuring conformational changes of biological macromolecules via such experiments. Measurements of conformational changes via spFRET are discussed elsewhere.[11,27−30]

Before discussing *single*-molecule transition dipoles, we summarize below how fluorescence polarization studies of *ensembles* of molecules are being used to extract information about the size, shape, and flexibility of macromolecules. In particular, steady-state and time-resolved fluorescence polarization anisotropy are used to study rotational dynamics of macromolecules.[32] To describe the light emission process, each fluorophore can be approximated by an absorption and emission transition dipole moments, $\vec{\mu}_a$ and $\vec{\mu}_e$, respectively. For the

* To whom correspondence should be addressed.
† Material Sciences Division.
‡ Physics Department.
§ Physical Biosciences Division.
|| Present address: Physics Department, Stanford University, Stanford, CA 94305.
▽ E-mail: tjha@stanford.edu, sweiss@lbl.gov.

10.1021/jp990948j CCC: $18.00
Published on Web 08/03/1999

rest of this report, unless otherwise noted, we assume $\vec{\mu}_a \parallel \vec{\mu}_e$ and denote the transition dipole by $\vec{\mu} = \vec{\mu}_a = \vec{\mu}_e$. This is the case for many common fluorophores. (We will show in section IIIA, however, that this relation does not hold for the molecule Cy5.) The absorption and the emission of photons are both polarized along the instantaneous direction of $\vec{\mu}(t)$. When linearly polarized light is used for excitation, only a subset of molecules, with dipoles aligned mostly along the excitation polarization, is selected from the ensemble (photoselection). The degree of polarization anisotropy in the emission, defined as $r = (I_{\parallel} - I_{\perp})/(I_{\parallel} + 2I_{\perp})$, with $I_{\parallel}$ the emission intensity along the excitation polarization and $I_{\perp}$ the emission intensity perpendicular to the excitation polarization, is a standard measure for the molecular motion of the system. For a rigid system, with molecules "frozen" in place, the emission will be predominantly polarized along the excitation polarization and r acquires its maximum steady-state value of 0.4.[32] For molecules in solution, however, a considerable amount of rotational diffusion during the excited-state lifetime results in the depolarization of the emission ($0 < r < 0.4$). Thus, steady-state measurements of $I_{\parallel}$ and $I_{\perp}$ provide information on the average amount of molecular rotational diffusion clocked by the emission lifetime. Polarization anisotropy studies can provide local information on viscosity and molecular level interactions that strongly influence rotational diffusion.

When the molecular rotation is anisotropic, that is, either if it is restricted to a certain cone angle, or if it has multiple time scales, the average anisotropy value obtained by a steady-state measurement can be misleading. To remedy this, time-resolved measurements are used to decouple the rotational time scale from the spatial rotational anisotropy. If the sample is excited by a short laser pulse, the evolution of $I_{\parallel}(t)$ and $I_{\perp}(t)$ in time, and therefore of $r(t)$, can be measured. Early photons, emitted immediately after excitation, are mostly aligned with the excitation polarization. Later photons are depolarized because enough time has elapsed to cause considerable amount of rotational diffusion. Therefore, $r(t)$ will decay from initial (maximum) value. The decay curve will exhibit multiple exponentials if several different dynamical processes are responsible for depolarization. A nonzero asymptotic value of $r(t)$ at very long times indicates restricted angular motion.

The photoselection process is eliminated altogether when a single fixed dipole is probed at a time. Güttler et al. measured the dipole of a single pentacene molecule in *p*-terphenyl at cryogenic temperatures.[33] Betzig and Chichester measured the orientation of the absorption transition dipole moment of single dye molecules at room temperature using polarized excitation light in the near-field.[2] These measurements were done with fixed excitation polarization and evoked Bethe theory[34] for the calculation of the light emanating out of the near-field aperture. The dipole approximation was then utilized to extract dipole orientation. Macklin et al. demonstrated imaging and emission lifetime spectroscopy of immobilized single molecules in the far-field, using laser scanning confocal microscopy.[10] They have shown that by imaging the same field-of-view with two orthogonal excitation polarizations, the in-plane component of the molecular dipole moment can be determined, and that by using higher order spatial beam profile, the $\hat{z}$ component of the molecular dipole can be determined as well.[35] Sepiol et al. showed that the $\hat{z}$ component of the emission dipole can be determined by the asymmetry of the collecting optics.[36] Dickson et al. showed that the three-dimensional dipole orientation can also be determined using the polarized evanescent fields generated in total internal reflection and the aberrations encountered in using oil immersion objectives focused into aqueous media.[37]

Depending on the molecular environment, the dipole may frequently reorient itself. Such reorientations may be responsible for fluorescent intensity fluctuations as was suggested by Ambrose et al. for rhodamine on a quartz surface.[3] Xie et al. tested this hypothesis on sulforhodamine 101 deposited on a dry glass surface by alternating the laser polarization and concluded that reorientations were not responsible for the observed fluctuations in their system.[5] On a slower time scale of hours, molecules can indeed reorient their dipoles as was shown for diI molecules embedded in polymer matrix by successive near-field imaging.[19] The rotational mobility of single fluorophores embedded in supported phospholipid bilayers was measured through polarization response and determined to be absent for that system.[38] We also found that reorientations are very rare on dry surfaces[13] but become much more frequent when the immobilized fluorophores are put into liquid.[24]

Exciting new biologically important measurements that use single molecule polarization spectroscopy are emerging. Axial rotation of an actin filament interacting with myosin molecules immobilized on a surface was directly visualized by video microscopy of single fluorescent molecules attached to the actin fiber.[20] Myosin conformational states were determined by the temporal changes in the rotational profile of a single fluorophore.[25] We were able to distinguish the inhibitor bound state from the free state of the enzyme staphylococcal nuclease (SNase) by studying the polarization response of a single fluorophore tethered to the enzyme.[27,28]

In this review, we describe various single-molecule imaging and spectroscopic techniques that utilize fixed or modulated polarized excitation and analyzed emission of single dipoles. It is shown that the dipole orientation and dipole orientation changes can be measured with high angular and temporal accuracy. Moreover, we show that the rotational dynamics of a single fluorophore, and therefore its rotational freedom of motion, can be determined. In contrast to conventional fluorescence polarization studies which are based on ensemble measurements, polarized single-molecule spectroscopy provides additional information on molecular motion which cannot be retrieved by steady state ensemble studies: it provides additional information on the hindered motion of the fluorophore. Our studies show that the dipole orientation is strongly affected by its local environment, therefore making it an ideal probe for the study of interactions between biological macromolecules, as clearly demonstrated in single-molecule polarization studies of fluorescently labeled proteins.

II. Materials and Methods

A. Sample Preparation. Typical sample preparation includes conjugation of fluorophores such as Texas Red (TR), tetramethylrhodamine (TMR), and Cy5 to the 5′ end of single strands of DNA molecules (10−20 bases long) through a flexible six-carbon chain and subsequent hybridization to the complementary strands. A glass coverslip is cleaned in 5% HF (hydrofluoric acid) solution to remove impurities and is treated with 2% aminopropylsilane solution. Dilute DNA solution (1 μL) (with concentration of 1−10 nM) is spread on the coverslip and then washed away with distilled water. This procedure ensures the adsorption of the DNA−fluorophore complex onto the silanized surface.[11] The coverslip is mounted directly on the sample scanner for experiments performed on dry surfaces or mounted into a liquid cell for experiments performed in aqueous conditions. For diffusion studies of fluorescently labeled

proteins, a dilute solution of protein is sandwiched between two HF-cleaned coverslips (the cleaning eliminates nonspecific binding of the protein to the surfaces). For polarization studies of immobilized proteins, coverslips are cleaned with acetone and methanol followed by water rinse. This provides the means to nonspecifically bind proteins to the coverslip's surface. Results obtained for proteins specifically bound to the surface via a histidine tag are reported elsewhere.[27,28]

B. Experimental Setup. A home-made scanning confocal microscope is used for the measurements. The excitation light is delivered through a single-mode optical fiber to the epi-illumination port. The laser beam has the following optical path: computer controlled shutter(Uniblitz, Vincent Associates, D122), $\lambda/4$ and $\lambda/2$ wave plates(CVI lasers) for precompensation of the fiber birefringence, single-mode optical fiber, computer controlled electrooptic modulator(ConOptics, M-350), $\lambda/4$ wave-plate (CVI lasers), a laser line filter (Omega optics). The modulator enables the rapid sweep of the polarization synchronized with the data acquisition. Samples are mounted on a piezotube scanner. Photons are collected with 1.3 or 1.4 numerical aperture (NA) oil immersion, infinity corrected objective (Zeiss, 100x Neofluor). The path of the fluorescent photons in the body of the microscope consists of the following: (i) color glass filter and/or dichroic mirror for excitation rejection (Omega Optics), (ii) tube lens, and (iii) pinhole. After the pinhole, the light is directed to one or two silicon avalanche photodiodes (APD, EG & G Canada, SPCM-200), used for acquiring images and emission time traces from single molecules. For the analysis of the emission polarization, a computer-controlled stepper-motor stage rotates the analyzer. A broadband polarizing beam-splitter cube(CVI laser) is used to project the two orthogonally polarized emission components onto the two APDs. A MS Windows based C++ computer program is used for imaging, automatic search, positioning and modulation spectroscopies.[13,39−41]

III. Results and Discussion

A. Immobilized Dipoles at the Glass-Air Interface. Fluorescence images of single dye molecules adsorbed on a dry glass surface were obtained by scanning confocal microscopy(images not shown). The images were acquired by scanning the sample stage with respect to the confocal excitation spot and recording the molecular emission for each sample position. Since the physical dimensions of a single molecule are much smaller than the excitation spot size, the molecule acts as a point source of light which maps the electric field distribution of the confocal spot.

Once such images are acquired, single molecules can be individually addressed by positioning them in the laser confocal spot. In Figure 1, an emission time trace (solid black line) from a single Texas Red (TR) molecule is recorded while the excitation polarization is repeatedly modulated from 0° to 90° (dotted line). Each sweep contains 91 points (1° increments) with 10 ms integration at each point. The intensity of the emission signal $F(t)$ is proportional to the absorption, which, according to the dipole approximation, is $F(t) \propto |\vec{\mu}\cdot\vec{E}(t)|^2$ where $\vec{\mu}$ is the molecular transition dipole and $\vec{E}(t)$ is the laser field. The data acquired at each polarization sweep can therefore be fit with $I_0 \cos^2(\alpha-\phi_0) + c$, where α is polarization angle, I_0 is the signal intensity, ϕ_0 is the in-plane dipole angle, and c is the background. We found that fitting parameters to individual consecutive sweeps varied very little, indicating a fixed orientation of the dipole. To improve the accuracy, the fitting was done on an average of the first four periods, as shown in the inset

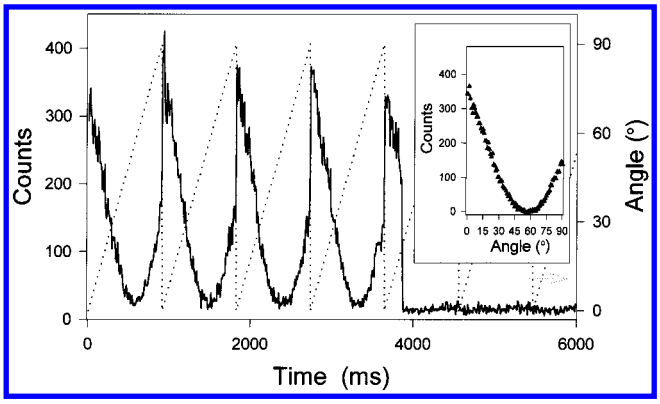

Figure 1. Fluorescence time trace of a single TR molecule (solid line) and the instantanous excitation polarization angle (dotted line). The inset shows the averaged signal of the first four periods (filled triangles) and a fit to $a\cos^2(x-b)+c$ (solid gray line). Reprinted with permission from ref 13. Copyright 1996 American Physical Society.

(black triangles). In the fifth period, the molecule photobleached. A best fit to the data is shown in solid gray line. The cosine square behavior with close to 100% modulation depth (the minima in the individual scans are slightly higher than the background level which is measured after photobleaching: this small component is most probably due to the residual birefringence introduced by the objective or dichroic mirror) and the sudden and complete drop of the emission to the background level (photodestruction) indicate a *fixed* orientation of a *single* dipole. The excellent fit not only allows us to determine the in-plane dipole orientation with great accuracy(0.2°), but is also a direct confirmation of the dipole approximation.

The measurement of Figure 1 probes the in-plane component of the absorption transition dipole $\vec{\mu}_a$ of a fixed fluorophore. It is also possible to probe the in-plane component of the emission transition dipole $\vec{\mu}_e$ by analyzing the polarization of the emitted light.[2] This was done by introducing an analyzer, mounted on a computer controlled rotational stage, in front of the APD detector. Data were collected in the following way: first, a molecule was located using the automated search. Then, a single period of excitation polarization sweep was performed to determine the absorption dipole orientation. Second, the laser polarization angle was set to be parallel to the determined absorption dipole. Then, several periods of analyzer angle sweeps were performed. To minimize the photobleaching, the laser excitation was blocked while the analyzer was moving between data points.

Figure 2a shows single Cy5 molecule emission intensity both as a function of the excitation polarization and as a function of the emission analyzer angle. Also shown are the fits to the cosine square function to determine the phase difference between the two. The nonzero minimum value, which is the result of depolarization from the high NA objective (Section IIIB) is substracted, and the two curves are normalized to the same maximum value. As can be seen, there is a phase shift between the two curves, suggesting that the absorption dipole and emission dipole are not collinear. This angular difference $\Delta\theta$ between the in-plane projections of the absorption and the emission dipoles was measured for 15 molecules. The resulting distribution in $\Delta\theta$ is shown in Figure 2b. The distribution has two peaks which are symmetrically displaced from $\Delta\theta = 0$ by about 5°. Since the absorption and the emission dipoles are fixed structural properties of the molecule, the sign of $\Delta\theta$ indicates the orientation (buttered side up or buttered side down) of the adsorbed molecule on the surface. The symmetry of the distribution indicates that the adsorption affinity is the same

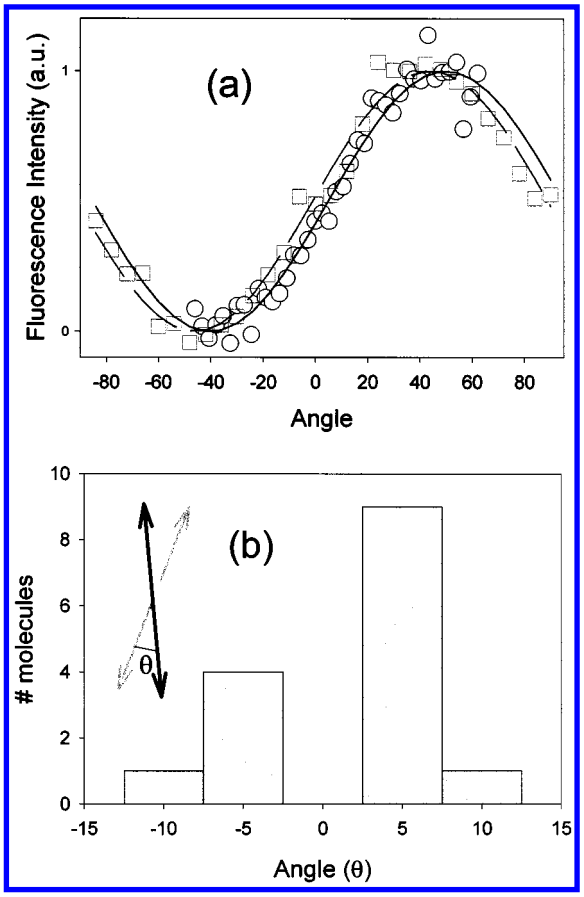

Figure 2. (a) The average fluorescent intensity of an immobilized Cy5 molecule as a function of the laser polarization angle (black circles) and the emission analyzer angle (gray squares). (b) Histogram of $\Delta\theta$ for 15 molecules showing a bimodal distribution.

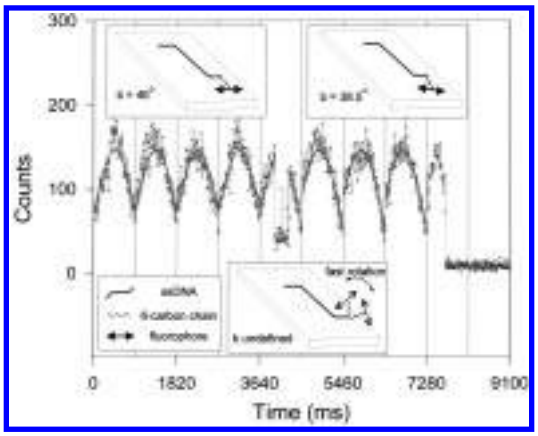

Figure 3. A 7.5° in-plane rotational jump of a TR molecule. Solid line is the fit to the data before and after the interruption. Vertical lines separate each modulation period from 0 to 90°. Insets show a model for the rotational jump. Reprinted with permission from ref 13. Copyright 1996 American Physical Society.

for both orientations. The absence of molecules with $\Delta\theta = 0$ suggests that the molecules lie flat on the surface.

In some rare cases, molecules on dry surfaces displayed rotational jumps that changed the dipole orientation. Figure 3 shows an emission time trace of a TR−DNA molecule, measured with a single detector. For the first four polarization scans, the dipole orientation is static. In the fifth scan, there is an interruption in the molecular emission. After this interruption, the emission signal resumes its initial value, but the phase of the signal changed. By fitting the data, it was found that the

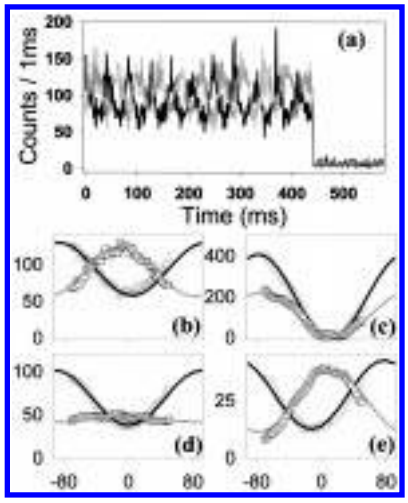

Figure 4. (a) Simultaneously obtained time traces of single molecules rapidly rotating in liquid. Excitation polarization is swept repeatedly over 120°, and the signal is measured in two orthogonally polarized channels. (black line for I_s and gray line for I_p.) (b) Time-averaged and background-subtracted signal for the raw data of (a) in circles (I_s) and squares (I_p). Best fits according to a model calculation are shown in black and gray lines. c−e are same as (b) measured on other three molecules. Reprinted with permission from ref 24. Copyright 1998 American Physical Society.

molecule changed its in-plane dipole orientation by 7.5 ± 0.4°. Because the peak intensity remained the same, we deduce that the out-of- plane dipole component did not change.

All of the very infrequently observed rotational jumps, including the one shown in Figure 3, displayed a transition period in the molecular emission (0.1−1.3 s long) that showed up as an interruption in the well-behaved series of sinusoidal curves. The explanation given at the time for the nature of these transition periods was desorption and readsorption of fluorophores onto the surface (see insets in Figure 3). As shown in the next section, single-molecule polarization modulation spectroscopy performed in aqueous conditions confirmed this interpretation.

B. Rotating Dipoles at the Glass−Water Interface. In this section we describe measurements done with aqueous buffer added to the sample. The addition of water caused the fluorescent molecules to frequently detach from the surface, and rapidly rotate around the six-carbon tether, likely due to the reduced binding affinity as a result of hydration. However, because the fluorophores were still anchored to the surface via the binding of the DNA to the silanized surface, they could not diffuse away and stayed within the excitation volume. This arrangement is ideal for the investigation of rotational diffusion kinetics of single molecules. It is worth noting that many in-vitro biological experiments are performed under similar conditions.

Typical polarization measurements in solution are shown in Figure 4. A polarizing beam-splitting cube separates the fluorophore's emission into two orthogonally polarized components (I_s and I_p, $\hat{s}$ and $\hat{p}$ axes are defined relative to the cube). Figure 4a shows raw data of simultaneously obtained emission time traces (I_s in black and I_p in gray) of a single rapidly rotating molecule. The single molecule nature of the signal is evident from the abrupt photobleaching at 442 ms. Figure 4b shows the same data as in Figure 4a, background subtracted and 11 periods averaged. The $\hat{x}$ axis is converted to the laser polarization angle, measured relative to $\hat{p}$ polarization. Figure 4c−e show similarly processed data (background subtracted and few periods

averaged) for another three individual molecules. In all figures I_s is denoted by empty circles and I_p is denoted by empty squares.

In general, each of the signals follows a $\cos^2(\theta)$ curve with a nonzero base line. When the molecule is immobilized, the two curves, I_s and I_p, have the same phase and 100% modulation depth; that is, the signal goes all the way to zero when the laser field is perpendicular to the in-plane dipole. An example for an immobilized dipole is shown in Figure 4c. The in-plane dipole orientation can be determined from the phase angle of the time traces with respect to the rotating excitation angle.[13] This phase angle determines the splitting ratio between I_s and I_p in this case.

However, when the fluorophore is rapidly rotating, a dramatically different relationship exists between the two curves. The two traces are approximately 180° out of phase, as is clearly shown in Figure 4a,b,d, and e. The reason for this remarkable difference is the photo-selection process. During fast rotation, the excitation is most effective when $\vec{\mu} \parallel \vec{E}$. Therefore, as long as the rotational diffusion is slower or comparable to the emission lifetime, the emission will be mostly polarized along $\vec{E}$. For example, if $\vec{E} \parallel \hat{s}$, $I_s > I_p$. Likewise, if $\vec{E} \parallel \hat{p}$, $I_s < I_p$. Therefore, the photoselection process results in the observed anticorrelation (180° phase shift) between the two signals.

The modulation depth is less than 100% because of the incomplete photoselection. It decreases as the rotational diffusion becomes faster. The small but noticeable deviation from the 180° phase shift in Figure 4b is due to hindered rotation. Since the phase shift between I_s and I_p for the two extreme cases are 0° for completely hindered rotation (immobilized fluorophore) and 180° for free rotation, it is quite obvious that hindered rotation of any intermediate degree would result in a phase shift between 0° and 180°.

Below, we present a simple model that allows us to quantitatively determine the degree of hindered rotation and the rotational time scale of single molecules. In order to clarify the assumptions made in our model, we start with general expressions and specify conditions to obtain the equations we will actually solve. We provide calculations of the depolarization effects of a high NA objective. Here, we only use them to estimate the potential for systematic errors. However, it also provides the basis for a more in depth study of high NA effects and will be the subject of a future paper. This model was presented in a previous paper,[13] but here we will discuss the model in more detail. Throughout the discussion, we use a coordinate system where $\hat{z}$ is the optical axis of the microscope pointing from the objective to the focus, and $\hat{x}$ and $\hat{y}$ are in the focal plane.

We first discuss the effects of the optical system on the excitation polarization. For a high NA objective, it is not possible to accurately describe the electromagnetic fields in the region of the focus with scalar diffraction theory. It is necessary to account for the vector nature of light. Richards and Wolf calculated the electromagnetic fields in the focal plane for an aplanatic system of angular semiaperture $\theta_{obj} = 60°$, where the incident field is a plane wave linearly polarized along the $\hat{x}$ axis.[43] For an objective using immersion oil with index of refraction $n = 1.52$, this corresponds to NA $= n \sin(\theta_{obj}) = 1.32$. We recalculated their results for an objective with NA $= 1.4$ ($n = 1.52$ and $\theta_{obj} = 66°$) using the method of Rishi Kant, and found nearly identical results to Richards and Wolf, with only slight differences in the numerical values.[45] In the focal plane, one finds that the polarization is $\hat{\epsilon} = E_x\hat{x} + E_y\hat{y} + iE_z\hat{z}$, where $E_{x,y,z}$ are positive real components of the polarization vector normalized so that $\hat{\epsilon}\cdot\hat{\epsilon}^* = 1$. The polarization ellipse is *perpendicular* to the focal plane. Two quantities of interest are $\chi = \tan^{-1}(E_y/E_x)$, and $\rho = |E_z|/\sqrt{|E_x|^2+|E_y|^2}$. χ is the angle between the $\hat{x}$ axis and the plane of the polarization ellipse, and ρ is the ratio of the z component of the electric field to the component within the focal plane. For a low NA system, one obtains $\chi = \rho = 0$. For high NA, this is true at the focus, but not in the adjacent regions. For NA $= 1.4$, within 2 optical units ($\upsilon = [2\pi/(\lambda/n)]\sqrt{x^2+y^2}\sin\theta_{obj}$) of the focus, the energy density drops by 50% or a little more depending on the direction of movement. Inside this area, χ varies by ±5°, and ρ is as high as 0.5 on the x axis. For vacuum wavelength $\lambda = 514$ nm (we often use this wavelength) and $\theta_{obj} = 66°$, 1 optical unit corresponds to about 60 nm.

As discussed elsewhere (ref 40), we optimize the position of the molecule for the maximum intensity. This normally corresponds to positioning the molecule as close to the focus as possible, where the field is closest to being purely polarized along the x axis. However, small errors in positioning (about 50 nm, the approximate step size in our search) may lead to z components 20% of the magnitude of the x components. In the focal plane, this error has the form $z_{err} = I_z^{max}(\upsilon)\cos(\phi)$, where ϕ is the angle from the x axis in the $x-y$ plane (see ref 43, eq 3.10). So, for the sake of later arguments, we use $I_z^{max}(\upsilon) = 0.2$ to discuss the z excitation effects. We define the angle α to be the angle between the x axis and the polarization of the excitation light. On the basis of the discussion above, the polarization of the excitation field for the single molecules is

$$\hat{x}_{exc} = \begin{pmatrix} \sqrt{1-z_{err}^2}\cos\alpha \\ \sqrt{1-z_{err}^2}\sin\alpha \\ iz_{err} \end{pmatrix} \quad \text{with} \quad z_{err} = I_z^{max}(\upsilon)\cos(\phi-\alpha)$$

We call the polarization along the x direction ($\alpha = 0$) $\hat{p}$ polarization, and along the y direction ($\alpha = \pi/2$) $\hat{s}$ polarization.

The absorption and emission interactions of single fluorescent molecules with the electromagnetic field can generally be modeled as interactions with electric dipoles. Define a spherical coordinate system with angle θ from the z axis and angle ϕ from the x axis in the $x-y$ plane. The absorption and emission dipole orientations are then defined as

$$\hat{\mu}_{abs} \equiv \hat{\mu} = \begin{pmatrix} \sin(\theta)\cos(\phi) \\ \sin(\theta)\sin(\phi) \\ \cos(\phi) \end{pmatrix} = \begin{pmatrix} x \\ y \\ z \end{pmatrix} \quad \text{and}$$

$$\hat{\mu}_{em} \equiv \hat{\mu}' = \begin{pmatrix} \sin(\theta')\cos(\phi') \\ \sin(\theta')\sin(\phi') \\ \cos(\theta') \end{pmatrix} = \begin{pmatrix} x' \\ y' \\ z' \end{pmatrix}$$

The rate of absorption is proportional to $|\hat{x}_{exc}\cdot\hat{\mu}|^2$, and the rate of emission is proportional to $|\hat{x}_{det}\cdot\hat{\mu}'|^2$, where $\hat{x}_{det}$ is a particular polarization direction that will be detected. Substituting in the expression for the excitation orientation, along with the dipole expression, we obtain

$$\begin{aligned} |\hat{\mu}\cdot\hat{x}_{exc}|^2 &= z_{err}^2\cos^2(\theta) + (1-z_{err}^2)\sin^2\theta\cos^2(\phi-\alpha) \\ &= [(1-I_z^{max}(\upsilon)^2)\sin^2(\theta) + I_z^{max}(\upsilon)^2\cos^2(\theta)] \times \\ &\qquad \cos^2(\phi-\alpha) + \frac{1}{4}I_z^{max}(\upsilon)^2\sin^2\theta\sin^2[2(\phi-\alpha)] \end{aligned}$$

The last term contributes a term to the absorption that has twice the frequency of the other terms. If z components were

important, we would see such a component in our data. Our data is very well fit without the higher frequency component, so we conclude that the last term is unimportant. Given the uncertainty in the position of the focus, the maximum $I_z^{max}(\upsilon)$ is 0.2, so

$$|\hat{\mu}\cdot\hat{x}_{exc}|^2 = [0.96\sin^2(\theta) + 0.04\cos^2(\theta)]\cos^2(\phi-\alpha) + 0.01\sin^2(\theta)\sin^2[2(\phi-\alpha)]$$

It is clear from the above expressions that, for fixed dipoles at high NA, we expect the absorption to drop to zero at $\phi - \alpha = (n + 1)(\pi/2)$. If it does not, then we expect that the dichroic mirror in use, the objective, or the interface is causing some depolarization of the excitation light. The high NA effects discussed so far have not changed the excitation field extensively from what we would expect from low NA theory, so we set $z_{err} = 0$ for the remainder of the paper,

$$|\hat{\mu}\cdot\hat{x}_{exc}|^2 = \sin^2(\theta)\cos^2(\phi-\alpha)$$

Next, we discuss the depolarization effects of the collected fluorescence emission. For a high NA objective, the rays imaged form a cone centered around the z axis with half-angle θ_{obj}. Each ray contributes some intensity to the p polarization and some to the s polarization. Upon refraction at an interface within the optical system, the angle between the ray polarization and the meridional plane (the plane defined by the z axis and the ray) remains approximately constant.[43] This is an approximation because of the polarization dependent transmission coefficients at interfaces. However, because microscope objectives are coated to reduce reflections the differences should be negligible. Axelrod computed the contribution to the p and s polarization for each ray and integrated the contributions over the light collection cone, and obtained the following results.[46] For a dipole orientation $\hat{\mu}$, with components (x,y,z), the contributions to the p and s polarizations are

$$I_p = I_{tot}(K_1x^2 + K_2y^2 + K_3z^2)$$

$$I_s = I_{tot}(K_2x^2 + K_1y^2 + K_3z^2)$$

where

$$K_1 = {}^3/_{32}(5 - 3\cos(\theta_{obj}) - \cos^2\theta_{obj} - \cos^3(\theta_{obj}))$$

$$K_2 = {}^1/_{32}(1 - 3\cos(\theta_{obj}) + 3\cos^2(\theta_{obj}) - \cos^3(\theta_{obj}))$$

$$K_3 = {}^1/_{8}(2 - 3\cos(\theta_{obj}) + \cos^3(\theta_{obj}))$$

These are slightly different from Axelrod's expressions, mainly in that they are normalized so that if $\theta_{obj} = \pi$ (i.e., an objective that collects all possible light),

$$I_s + I_p = I_{tot}(x^2 + y^2 + z^2) = I_{tot}$$

For the NA = 1.4 objective, $K_1 = 0.332$, $K_2 = 0.0065$, and $K_3 = 0.106$. With a low NA objective, K_1 dominates so an x component for a dipole directly corresponds to the intensity in the p detector, and a y component directly corresponds to the intensity in the s detector. For high NA, K_2 is still much less than K_1, so we ignore the mixing of polarization from the x and y components. However, K_3 is not small, and thus the z component of polarization is mixed in considerably. This effect is not taken into account in our current model, but we discuss the limits it imposes on interpretation of our calculations.

In the present work, we ignore the effects of the glass−water interface. However, for dipoles located at the interface, the radiation patterns are distorted significantly from the usual expressions for homogeneous media.[47−49] We also do not consider the polarization dependence of the dichroic beam splitter used in the epi-fluorescence setup.

Orientational dynamics of the fluorophores are modeled as follows. Prior to excitation, the molecule's absorption dipole has a normalized steady-state orientational probability density $U(\theta,\phi)\sin(\theta)d\theta d\phi$. This gives the probability that the absorption dipole is pointed in a certain direction (θ,ϕ) within the limits $d\theta$ and $d\phi$. Upon absorption of a photon at time $t = 0$, we need to know the probability density $V(\theta',\phi',t;\theta,\phi)\sin(\theta')d\theta'd\phi'$. This is the probability that the emission dipole is pointed in the direction (θ',ϕ') within the limits $d\theta'$ and $d\phi'$ at time t, given that the molecule was excited at $t = 0$ with the absorption dipole pointed in the direction (θ,ϕ). After sufficient time, the molecule loses memory of its initial state, and returns to the steady state density. For $\vec{\mu}_{abs}|\vec{\mu}_{em}$, as $t \rightarrow \infty$, this means $V(\theta',\phi',t;\theta,\phi) \rightarrow U(\theta',\phi')$. Also, we need to know the probability density $f(t)\,dt$, the probability that the molecule will emit a photon at time t after excitation. We assume a single exponential behavior with lifetime τ, $f(t) = e^{-t/\tau}/\tau$. Given these probability densities, the intensity detected along $\hat{x}_{det}$ for an excitation polarization $\hat{x}_{exc}$ is

$$I(\hat{x}_{exc},\hat{x}_{det}) = \text{const}\int_0^\infty dt\int_{-1}^1 d\cos(\theta)\int_0^{2\pi} d\phi\int_{-1}^1 d\cos(\theta')\int_0^{2\pi} d\phi'\,|\hat{\mu}'\cdot\hat{x}_{det}|^2\,V(\theta',\phi',t;\theta,\phi)|\hat{\mu}\cdot\hat{x}_{exc}|^2U(\theta,\phi)\frac{e^{-t/\tau}}{\tau}$$

where "const" contains many factors such as the molar extinction coefficient, the laser intensity, quantum efficiency of the dye, efficiency of the detectors, etc. $\hat{x}_{det}$ is given by

$$\hat{x}_{det} = \begin{pmatrix}\sin(\theta_{det})\cos(\phi_{det})\\ \sin(\theta_{det})\sin(\phi_{det})\\ \cos(\theta_{det})\end{pmatrix}$$

We assume that the density V returns to the steady-state density U before the molecule is re-excited. We can make one additional observation about the general response equation above. Given the model we have for the absorption and emission dipoles, and the excitation and detection schemes, the response at each detector can be modeled by a function of the form $I_{det} = a_1 + a_2\cos^2(\alpha-\alpha_3)$. This can be seen easily by expanding out the trigonometric terms for the excitation response and pulling the terms involving α outside the integral. These terms can then be regrouped to form a function of the form just mentioned. This of course puts significant constraints on how much information can be obtained by this method. There may be a whole class of distributional models that fit the data.

It is possible to solve more complicated models, but, to make the calculation simpler, we consider the case of a dipole rotating in the plane with reflecting boundary conditions.[42] The single fluorophore is modeled by simple linear diffusion of a rapidly rotating dipole moment within a wedge in the focal plane (Figure 5). Since the measurement is sensitive mostly to the in-plane component of the dipole, the approximation may be quite good as long as the projection to the plane is properly accounted for (see below). The dipole is allowed to rotate in the $\hat{s} - \hat{p}$ plane and makes an angle ϕ relative to $\hat{p}$ (see Figure 5). The dipole is assumed to have a fixed z component; it makes a constant

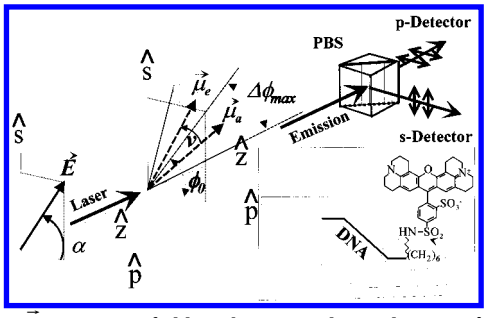

Figure 5. $\vec{E}$, excitation field, makes an angle α relative to $\hat{p}$. $\hat{z}$ is the propagation direction for the exciting field and the collection axis for the fluorescence emission. $\vec{\mu}_a$ and $\vec{\mu}_e$ are the molecular dipole moments for absorption and emission. v represents the rotational diffusion during the excited-state lifetime. The dipole moment is constrained to a cone with a center angle ϕ_0 and a half-cone angle $\Delta\phi_{max}$. The collected emission is split by a polarizing beam splitting cube (PBS) and the two signals, I_s and I_p are simultaneously recorded. The inset shows the chemical structure of the dye−DNA complex and the linker region. Reprinted with permission from ref 24. Copyright 1998 American Physical Society.

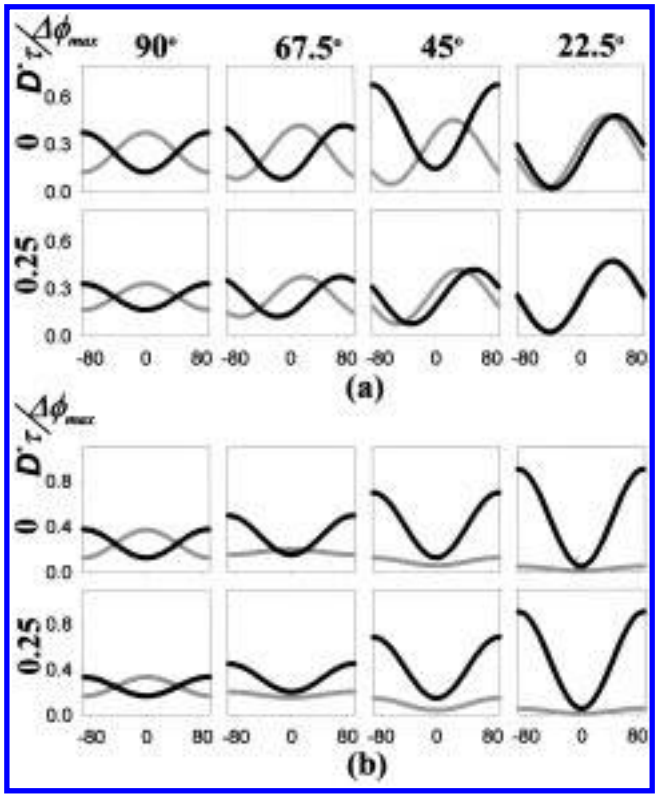

Figure 6. Results of simple model calculation for the $I_s(\theta)$ (black) and $I_p(\theta)$ (gray) for given excitation angle θ, rotational diffusion parameter $D^*\tau$, center angle ϕ_0, and half-cone angle $\Delta\phi_0$. ϕ_0 is 45° for (a) and 0° for (b). Reprinted with permission from ref 24. Copyright 1998 American Physical Society.

angle θ_0 from the optical axis. A dipole entirely in the plane corresponds to $\theta_0 = 90°$. In contrast to polarization anisotropy measurements on ensemble of fluorophores in solution, the interaction of the tethered fluorophore with the DNA molecule and more importantly with the glass surface can limit the range of ϕ. It is assumed that the dipole is rotating around the angle ϕ_0, with a half-wedge-angle in the plane, of $\Delta\phi_{max}$: $\phi_0 - \Delta\phi_{max} < \phi < \phi_0 + \Delta\phi_{max}$. It is further assumed that (i) the dipole can be found anywhere within this range of angles with identical probabilities (this is the result of the reflecting boundary conditions, and that (ii) $\vec{\mu}_{abs} || \vec{\mu}_{em}$ in the absence of rotational diffusion. What these assumptions mean for the above general expressions is that

$$U(\theta,\phi) = u(\phi)\delta(\theta-\theta_0), \quad \text{where}$$

$$u(\phi) = \begin{cases} \dfrac{1}{2\Delta\phi_{max}} & \text{for } \phi_0 - \Delta\phi_{max} < \phi < \phi_0 + \Delta\phi_{max} \\ 0 & \text{otherwise} \end{cases}$$

and

$$V(\theta',\phi',t;\theta,\phi) = v(\phi',t;\phi)\delta(\theta'-\theta_0)$$

where v satisfies

$$\frac{\partial v}{\partial t} = D^*\frac{\partial^2 v}{\partial \phi'^2}$$

with the boundary conditions

$$\left.\frac{\partial v}{\partial \phi}\right|_{\phi'=\phi_0-\Delta\phi_{max}} = \left.\frac{\partial v}{\partial \phi'}\right|_{\phi'=\phi_0+\Delta\phi_{max}} = 0$$

and initial conditions

$$v(\phi',t=0;\phi) = \delta(\phi'-\phi)$$

It is convenient to introduce a change of variables

$$x = \phi - (\phi_0 - \Delta\phi_{max})$$

$$y = \phi' - (\phi_0 - \Delta\phi_{max})$$

and define

$$x_0 = \alpha - (\phi_0 - \Delta\phi_{max})$$

$$y_0 = \phi_{det} - (\phi_0 - \Delta\phi_{max})$$

$$L = 2\Delta\phi_{max}$$

In terms of these variables, our overall expression is

$$I(\hat{x}_{exc},\hat{x}_{det}) = \text{const} \int_0^\infty dt \int_0^L dx \int_0^L dy \frac{1}{L} v(y,t;x)\frac{e^{-t/\tau}}{\tau} \times \cos^2(x-x_0)\sin^2(\theta_0)[\cos(\theta_0)\cos(\theta_{det}) + \sin(\theta_0)\sin(\theta_{det})\cos(y-y_0)]^2$$

The equation for v now is

$$\frac{\partial v}{\partial t} = D^*\frac{\partial^2 v}{\partial y^2}$$

the boundary conditions are

$$\left.\frac{\partial v}{\partial y}\right|_{y=0} = \left.\frac{\partial v}{\partial y}\right|_{y=L} = 0$$

and the initial condition is

$$v(y,t=0;x) = \delta(y-x)$$

We solve this equation by separation of variables and write the solution in terms of an eigenfunction expansion. Assuming $v(y,t) = g(t)h(y)$, we then obtain

$$g(t) = e^{-D^*\lambda^2 t} \qquad \text{and} \qquad \frac{d^2h}{dy^2} = -\lambda^2 h$$

The solutions to the second equation with the given boundary conditions are

$$h(y) = \cos(\lambda y) \qquad \text{for} \qquad \lambda L = n\pi \qquad \text{where} \qquad n = 0, 1, 2, \ldots$$

So, $v(y,t)$ can be expanded as

$$v(y,t) = A_0 + \sum_{n=1}^{\infty} A_n \cos\left(\frac{\nu\pi y}{L}\right) e^{-D^*(n\pi/L)^2 t}$$

Using $v(y,t=0;x) = \delta(y-x)$,

$$v(y,t;x) = \frac{1}{L}\left(1 + 2\sum_{n=1}^{\infty} \cos\left(\frac{n\pi y}{L}\right)\cos\left(\frac{n\pi x}{L}\right) e^{-D^*(n\pi/L)^2 t}\right)$$

Substituting this into the expression for I ($\hat{x}_{exc}$, $\hat{x}_{det}$) and performing the necessary integrations, we obtain for different detection directions,

$$I(\hat{x}_{exc}, \hat{z}) = \text{const}\,\frac{\sin^2(\theta_0)\cos^2(\theta_0)}{L}\left(\frac{L}{2} + \frac{1}{4}\sin 2(L - x_0) + \frac{1}{4}\sin(2x_0)\right)$$

$$I\left(\hat{x}_{exc}, \theta_{det} = \frac{\pi}{2}, \phi_{det}\right) = \text{const}\,\frac{\sin^4(\theta_0)}{L^2}\left[\left(\frac{L}{2} + \frac{1}{4}\sin 2(L - x_0) + \frac{1}{4}\sin(2x_0)\right)\left(\frac{L}{2} + \frac{1}{4}\sin(2)(L - y_0) + \frac{1}{4}\sin(2y_0)\right) + \sum_{n=1}^{\infty} \frac{1}{1 + \left(\frac{n\pi}{L}\right)^2 D^*\tau}\left(\frac{\sin(2L - 2x_0)(-1)^n + \sin(2x_0)}{4 - \left(\frac{n\pi}{L}\right)^2}\right)\right]$$

Because the above expressions are singular for the special case $L = (n\pi)/2$, these values need to be treated separately. However, we can also simply set L close to $(n\pi)/2$ if we do not want to recalculate these expressions.

The results are arranged in a table form, where plots of I_s and I_p as functions of laser polarization angle α are displayed for a few selected values of $D^*\tau$ and $\Delta\phi_{max}$. The table in Figure 6a was calculated for $\phi_0 = 45°$ and the one in Figure 6b for $\phi_0 = 90°$. $\theta_0 = 90°$ for these figures.

The product $D^*\tau$ (the effective rotational diffusion coefficient times the emission lifetime) is a measure of the rotational diffusion rate, and $\Delta\phi_{max}$ (the half cone angle) represents the degree of allowed rotation. Please note that $D^*\tau = 0$ for rotation much slower than τ, and $D^*\tau \gg 1$ for very fast rotation. Also, $\Delta\phi_{max} = 0$ for a fixed dipole and $\Delta\phi_{max} = 180°$ for free rotation. Notice that, due to the reflecting boundary conditions and the symmetry of the dipole absorption and emission, $\Delta\phi_{max} = 90°$ gives identical results to free rotation.

The results in the first column of Figure 6a ($\Delta\phi_{max} = 90°$, the same numerically as free rotation) are equivalent to the results obtained from traditional ensemble fluorescence depolarization measurements. The single, molecule fluorescence anisotropy r, given by $r = (I_s(\alpha = 90°) - I_p(\alpha = 0))/(I_s(\alpha = 90°) + 2I_p(\alpha = 0))$ has a value of 0.4 for $D^*\tau = 0$ (slowly rotating dipole), in analogy to a rigid system of many molecules "frozen" in place. The single molecule anisotropy approaches 0 for $D^*\tau \gg 1$ (rapidly rotating dipole), in analogy to an ensemble of rapidly rotating molecules. The top row in Figure 6 illustrates the effect of the rotational hindrance. Both the relative phase and the modulation depth change as $\Delta\phi_{max}$ changes from free rotation ($\Delta\phi_{max} = 90°$) to a fixed dipole ($\Delta\phi_{max} = 0$).

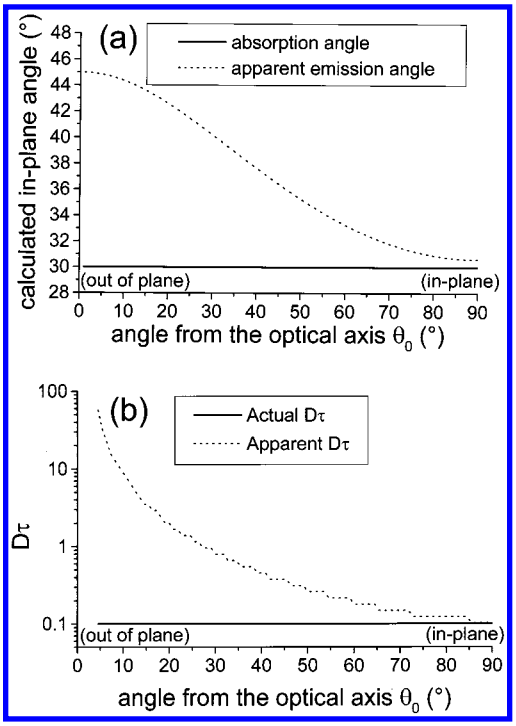

Figure 7. (a) The calculated in-plane emission angle as a function of θ_0 ($\phi_{em} = \tan^{-1}$ (total intensity on S detector/total intensity on P detector)$^{1/2}$ for a fixed dipole. The dipole is oriented so that $\phi_0 = 30°$. The effect of mixing $\hat{z}$ components of polarization into the detection is to shift the detected emmission angle toward 45°. (b) The value of the fit parameter $D\tau$ as a function of fixed θ_0 when the *real* value of $D\tau$ is 0.1 and $\Delta\phi_{max} = 180°$. ϕ_0 is irrelevant in this case, since the dipole is freely rotating in the plane.

With the help of the tables of Figure 6, it is possible to unambiguously determine ϕ_0, $\Delta\phi_{max}$ and $D^*\tau$ for the experimental data. For example, we can find closely matching profiles for the data of Figure 4b−e in Figure 4. In the following we detail the procedure used for the fitting.

We note that the sum signal $S(\alpha) = I_s(\alpha) + I_p(\alpha)$ does not depend on the rotational diffusion time scale as long as it is faster than the data acquisition time. The phase of the sum signal $S(\alpha)$ and its modulation depth $M_s = (S_{max} - S_{min})/(S_{max} + S_{min})$ directly determine ϕ_0 and $\Delta\phi_{max}$. Then $D^*\tau$ is varied, while allowing up to 20% imbalance between the two detectors, until a best fit to the data is obtained. The solid lines in Figure 4b−e are such best fits.

Rotational profiles determined using the above planar model should adequately describe the planar projection of the true 3D rotational diffusion in the absence of instrumental depolarization sources. However, in the presence of the depolarization, such a planar model can be misleading since emission from the z component of the dipole can be mixed into that of the planar components. Figure 7a shows the calculated emission angle as a function of θ_0 ($\phi_{em} = \tan^{-1}$ (total intensity on S detector/total intensity on P detector)$^{1/2}$ for a fixed dipole. The dipole is oriented so that $\phi_0 = 30°$. The effect of mixing z components of polarization in the detection is to shift the detected emmission angle toward 45°. For dipoles rotating freely in the plane, with fixed θ_0, the ratio between the modulation depth and the modulation offset varies considerably as a function of θ_0. These effects, if ignored, can skew the values of fitted parameters.

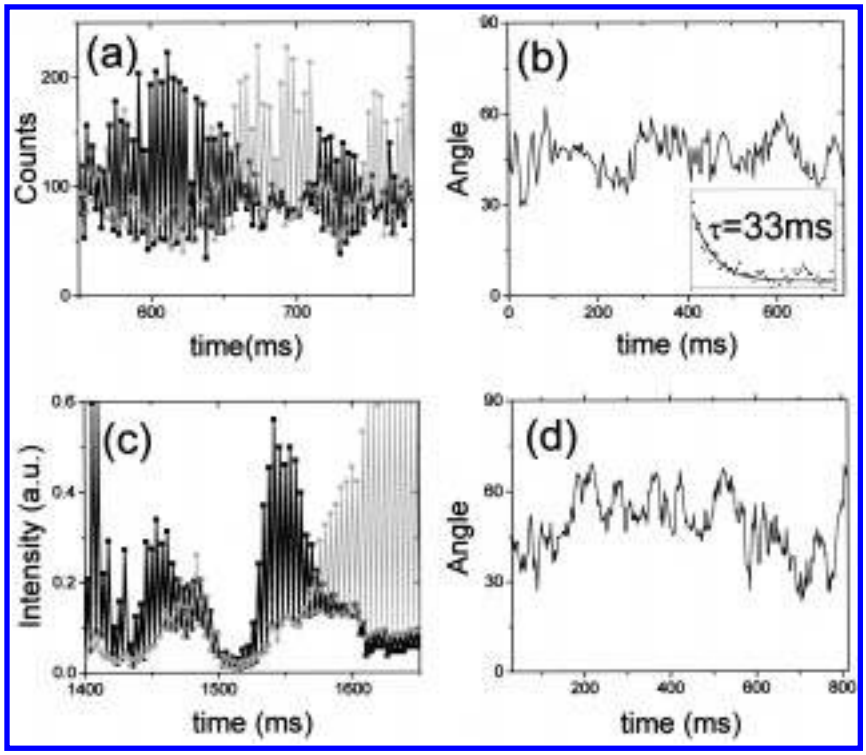

Figure 8. (a) Raw smFPA I_s (black) and I_p (gray) time traces. (b) Angle parameter calculated from (a). The inset shows an autocorrelation together with an exponential fit. (c) Simulated smFPA time traces. (d) Angle parameter calculated from (c).

For example, Figure 7b shows the value of the fit parameter $D\tau$ as a function of fixed θ_0 when the *real* value of $D\tau$ is 0.1 and $\Delta\phi_{max} = 180°$. The constraints imposed by these effects ought to be considered when analyzing polarization modulation data.

When the fluorophores are covalently linked to macromolecules, the rotations about the valence bonds can be limited by steric hindrances. We believe that the steric hindrance due to neighboring chemical groups, determined by the geometrical structure of the DNA molecule and the surface causes $\Delta\phi_{max}$ to be less than 180° for most of the studied molecules.

The data in Figure 4b indicates a freely rotating fluorophore while the data in Figure 4c indicates a fixed fluorophore. However, many fluorophores displayed a mixed behavior, where approximately half of the time they were fixed to the surface and half of the time they freely rotated. These transitions between the surface-bound and unbound states were discrete in time (termed here "rotational jumps") and were mainly caused by photoexcitation, with some small residual spontaneous term.[24]

We have demonstrated the ability to closely monitor rotational dynamics of single fluorophores. It was shown that single molecule fluorescence polarization anisotropy (smFPA) studies can provide detailed information on hindered rotational diffusion. The measurements presented here suggest that great care must be taken when interpreting ensemble anisotropy measurements of fluorophores that are strongly interacting with their immediate surroundings. Many immediate applications of this methodology include: (1) understanding the binding geometry of the fluorophore, macromolecule, and surface system, (2) direct observation of conformational changes of biological macromolecules undergoing biochemical reactions, (3) distinguishing the fluorophore's rotational dynamics from other molecular dynamics. For example, when inferring conformational changes of macromolecule by single-pair fluorescence resonance energy transfer.[11,27] it is essential to isolate orientational changes from distance changes. The orientations of the donor's and acceptor's dipoles strongly affect the efficiency of energy transfer, and as is shown here, the dipoles' rotational dynamics can be very significant. Lastly, it is noted that the smFPA technique can be easily extended to the time domain with two time-correlated photon-counting detection channels. This will allow the measurement of the time-resolved fluorescence polarization anisotropy signal of a single molecule on nanosecond time scale.[22]

C. Rotational Dynamics of Protein Conjugated Fluorophores on a Surface. Contrary to an early belief that proteins are rigid, solid-like entities, it is now widely accepted that even in the equilibrium state they undergo structural fluctuations governed by statistical thermodynamic principles. So far, conventional experimental techniques have yielded little direct evidence of such behavior. Single-molecule fluorescence polarization anisotropy (smFPA) measurements may report on these fluctuations if the interaction between the fluorophore and the protein is strong enough.

We have measured the polarization response of a single tetramethylrhodamine(TMR) fluorophore tethered to the enzyme Staphylococcal nuclease (SNase).[27] In the study presented here, SNase was nonspecifically adsorbed to a glass substrate in an aqueous solution containing 15% glycerol.

To measure the dipole effects in emission, I_s and I_p were simultaneously recorded on the two detectors. To measure the dipole effects in absorption, the excitation polarization was alternated between two orthogonal excitation polarizations, again parallel to $\hat{s}$ or $\hat{p}$. A set of four data points were taken consecutively at times n and $n + 1$: $I_{ss}(n)$, $I_{sp}(n)$, $I_{ps}(n + 1)$ and $I_{pp}(n + 1)$ where the first index denotes the excitation polarization, the second denotes the emission polarization. Many such data sets were taken repeatedly until the fluorophore photobleached. As was shown in the previous section for fluorophores tethered to immobilized DNA molecules, the time traces recorded in this manner are correlated for a fixed dipole but anticorrelated for a freely rotating dipole.

Typical time traces are shown in Figure 8a. The dipole gradually alternates between $\hat{s}$ and $\hat{p}$ directions showing an anticorrelated behavior in the interval between 630 ms to 660 ms and between 720 and 750 ms. The fluorophore was most likely not completely freely rotating nor was it fully immobile at any time. Thorough understanding of the rotation profile would require higher resolution measurements with more data points for different excitation polarization angles. The data is consistent with a fast, restricted rotational diffusion of the dipole within a cone, which itself is precessing (by a random walk) in time. Simulations based on these assumptions produce qualitatively similar data, as shown in Figure 8c. The restricted motion of the dipole and the dynamic changes are most probably due to steric interactions between the fluorophore and the protein and/or the surface. Although smFPA measurements do not directly report on the actual in-plane dipole orientation when the fluorophore is rotating, it is possible to define an effective average dipole angle parameter in the following way: $\theta_{em} = \tan^{-1}\sqrt{(I_{ps}+I_{ss})/(I_{sp}+I_{pp})}$. The angle parameter θ_{em} can be thought of as the average in-plane cone angle center of the rotating emission dipole measured with a circularly polarized light at the mid time point between n and $n + 1$. Figure 8b shows the time fluctuations of the angle parameter θ_{em} calculated from the data in Figure 8a. The fluctuations resemble a random walk with a time constant of $\tau_A = 33$ ms, as shown by the autocorrelation and fit in the inset. Even though there is a large distribution of τ_A among molecules, its distribution does not depend on the laser intensity, indicating spontaneous dynamics. We also compared the total intensity ($I_{ps} + I_{pp} + I_{sp} + I_{ss}$) fluctuations with the angle parameter fluctuations on each molecule and found that their time constants are within a factor of 2 of each other. This indicates that the fluorescence intensity fluctuation are mostly due to dipole rotational dynamics rather than spectral shifts or changes in quantum yields.

It is interesting to note that the fluctuations in dipole orientation of fluorophores bound to SNase are very different from those observed for fluorophores tethered to DNA. In the latter case, abrupt and infrequent (1−10 s time scale) orientational jumps due to discrete events of desorption and readsorption were observed.[24] These jumps originated, most probably, from light-induced fluorophore conformational changes. The dipole reorientations for SNase, however, were larger, much more continuous, on a faster time scale, and were not induced by light. Therefore, it is likely that the observed rotational fluctuations are protein related and are due to interactions between the protein, fluorophore, and the glass surface.

We performed numerical simulations based on a model where the dipole is rapidly rotating (on the time scale of the fluorescence lifetime) within a cone (with half cone angle 45°) combined with a random walk of the cone bisector angle on a much slower (millisecond) time scale. Figure 8c shows the simulated time traces at the two detectors and Figure 8d shows the simulated θ_{em} (as defined above). The model calculations are qualitatively similar to the experimental data.

Because the proteins were nonspecifically bound to the surface, we could not distinguish whether it is the fluorophore only or the whole protein that is precessing/tumbling. In fact, using histidine tag for specific immobilization greatly reduced the rotational dynamics, indicating that surface interactions must play a major role in the observed dynamics described above.[27] Rigid fixation of the fluorophore to the protein together with a specific immobilization of the whole complex to the surface would make it possible to study relative motion of subunits within a single protein molecule in real time.

D. Polarization Anisotropy of Protein Conjugated Fluorophores Diffusing in a Liquid. In analogy to ensemble fluorescence polarization anisotropy (FPA) measurements, single molecule anisotropies can be deduced from $I_{||}$ and $I_{\perp}$, measured for each burst of photons that is produced when a diffusing molecule traverses the laser excitation volume. Previously, anisotropy measurements using fluorescence correlation spectroscopy (FCS) were performed in diffusion.[50,51] We emphasize, however, that the single-molecule approach described below addresses one molecule at a time. Figure 9a shows photon bursts collected from single SNase molecules that are labeled with a single TMR molecule, diffusing in a buffer containing 15% glycerol and excited with 4×10^7 W/cm^2. Adjacent data points that obey $I_{||} + I_{\perp} > \bar{b} + 5\sigma_b$ with $\bar{b}$ and σ_b, being the average and the standard deviation of the total background counts, are grouped together and analyzed as a single burst. The integrated photon counts (background subtracted) measured at each detector for the ith burst are noted $I^i_{||}$ and $I^i_{\perp}$ respectively. The polarization anisotropy can be calculated for each individual burst i according to $r^i = (I^i_{||} - I^i_{\perp})/(I^i_{||} + 2I^i_{\perp})$. A large number of single-molecule anisotropy values can be collected to provide information on the distribution in the degree of rotational freedom of motion of the fluorophores. This is in contrast to the conventional FPA measurement that provides information only on the ensemble anisotropy average value: $\bar{r} = (\sum I^i_{||} - \sum I^i_{\perp})/(\sum I^i_{||} + 2I^i_{\perp})$. Because of anisotropy in the optical system itself, two data sets with two orthogonal laser excitation polarizations are collected. The anisotropy in the optical system is eliminated by requiring self-consistency for the $\bar{r}$s of both distributions. Figure 9b shows a 2D scatter plot of the corrected distribution of r^i vs $S^i = I^i_{||} + I^i_{\perp}$ (burst size). As can be seen, this distribution is broad and includes data points with negative r values, which are physically not valid (r can take any value between 0 and 0.4). This is mostly due to the low number of counts collected from single molecules and the resulting shot noise. Since the average value of r is only 0.02, small fluctuations can easily result in unphysical r values. In the discussion below we will focus our attention to the mean and standard deviation of the r^i distribution.

Let us, for the moment, consider the binding geometry of the fluorophore, through a flexible linker (six carbons in most cases), to the protein. Depending on the steric interactions at the binding site, the fluorophore's freedom of motion can vary all the way from rapid rotation relative to the protein via the segmental motion of the linker to full immobilization on the protein when strong interactions are present. Since the rotational diffusion time scale depends on the effective volume of the rotating particle (a rule of thumb for this time scale is one half of the molecular weight times picoseconds), the fluorophore will have two vastly different time scales for the two extreme cases. For a freely rotating fluorophore, the rotational time scale τ_r is 600(molecular weight of TMR)/2 = 300 ps while for the fully immobile fluorophore τ_r is 19,000(molecular weight of SNase)/2 = 9500 ps. The fluorescent lifetime τ_f of TMR is on the order of a few nanoseconds. For the freely rotating fluorophore, the large amount of rotational diffusion that the fluorophore undergoes within τ_f results in the loss of the original information about the excitation polarization and r will therefore approach zero. For the immobilized fluorophore case, the whole protein−fluorophore complex rotates slowly compared to τ_f, and much of the information about the excitation polarization will be retained with r approaching its maximum value of 0.4. Therefore, it should be possible to identify and separate the two types of sub-populations if r is measured on one protein at a

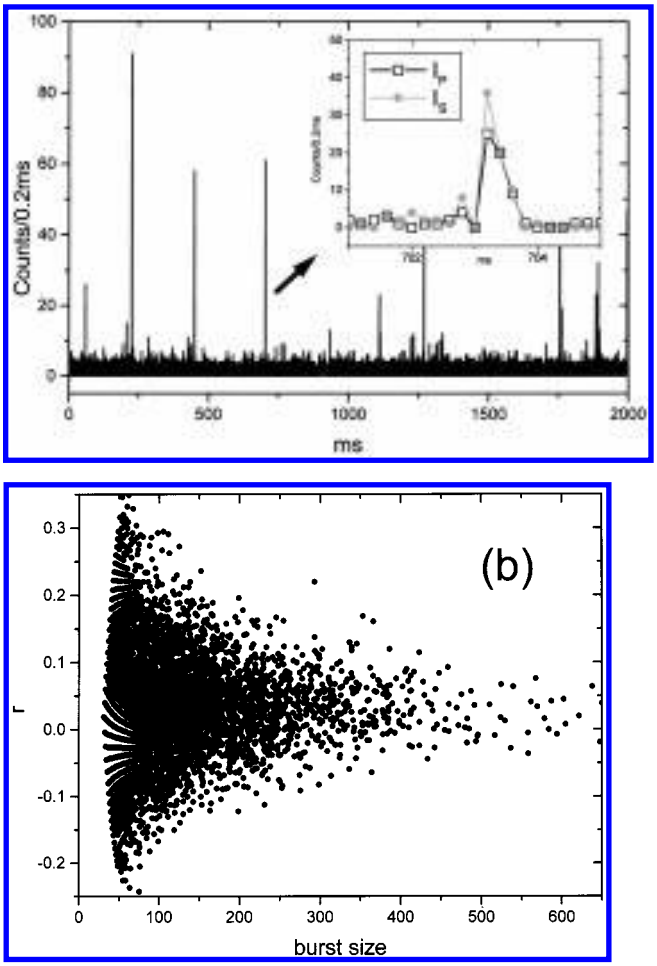

Figure 9. (a) A polarization time trace of data collected from diffusing moleculues. The sum S of the two signals ($I_s + I_p$) is shown. The inset shows the two signals independently (black for I_s and gray for I_p) for a small section of the data. (b) r^i vs burst size S^i.

time. We were in fact motivated by the results obtained from surface immobilized proteins (section III.C) where frequent changes in the rotational profiles were observed. If these frequent changes are not due to the immobilization of the proteins to the surface, it should be possible to distinguish between the two subpopulations ($r = 0$ and $r = 0.4$) of the freely diffusing proteins in solution, provided that other sources of noise do not broaden the distribution of r too much.

As can immediately be seen from Figure 9b, the scatter of r values is bigger for smaller burst size indicating that the shot noise plays a major role in the distribution width. The r values for data points with burst sizes between 100 and 200 total counts are shown in Figure 10. Three histograms were constructed from three different samples: TMR-labeled SNase in 15%, 60%, and 80% glycerol. Each histogram is fitted with a Gaussian distribution $e^{-2(r-\bar{r})^2/(\Delta r)^2}$ to extract $\bar{r}$ and the width Δr, except for the 80% glycerol case where two gaussian peaks were used to fit the data. As can be seen, $\bar{r}$ increases $0.03 \rightarrow 0.09 \rightarrow 0.14$ as the viscosity increases. (For the 80% glycerol case, the average value of the two extracted $\bar{r}$s is used). This viscosity dependence proves that the measurement truly reflects the rotational anisotropy on a single molecule level. Even though Δr is rather large (0.14 for 15% glycerol and 0.12 for 60% glycerol, fully accountable by shot noise only in the chosen burse size range), it would have been possible to identify a second peak around $r = 0.4$ if a substantial subpopulation of proteins with immobile fluorophores was present. The fact that

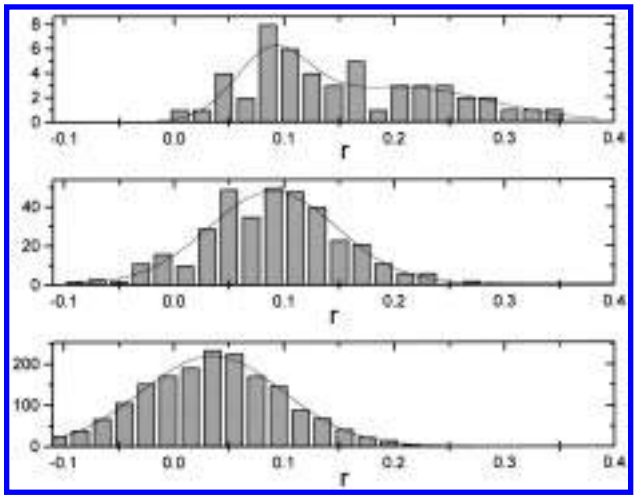

Figure 10. Distributions of single molecule fluorescence polarization anisotropy r for three different concentrations of glycerol: (a) 80%, (b) 60%, and (c) 15%.

the 80% glycerol case could not be satisfactorily fitted with only one Gaussian may be an indication of two distinct populations with two r values which are not very different. This last result is consistent with the results obtained from surface immobilized proteins: the effective viscosity near the water−glass interface is higher than the bulk viscosity. We therefore may expect fluorophores linked to surface immobilized proteins to have similar rotational characteristics as freely diffusing proteins in highly viscous liquid. We note that such a conclusion could not be drawn from conventional ensemble FPA studies.

So far we have ignored the depolarization effect due to the objective in the diffusion geometry. Koshioka et al. studied these effects.[44] They used a general model combined with experimental observations of time-resolved anisotropy decay to determine the depolarization effects of the collection optics. Below, we estimate the effect of using a high NA objective on r. Our expression is similar to that obtained by Koshioka et al. However, they measure an effect somewhat larger than we estimate. This is most likely due to additional depolarization effects in the light path. We define $I_{x,y,z}$ to be the intensity emitted by the dipole with the respective polarization along x,y, or z:

$$I_x = I_{\text{tot}}x^2, \quad I_y = I_{\text{tot}}y^2, \quad \text{and} \quad I_z = I_{\text{tot}}z^2$$

It is evident that

$$I_x + I_y + I_z = I_{\text{tot}}$$

The light detected by the detectors, as was discussed earlier, is a mixture of all three components:

$$I_p = K_1 I_x + K_3 I_z$$
$$I_s = K_1 I_y + K_3 I_z$$

Here, we assumed that $K_2 \ll K_1$, so we ignore mixing of I_x and I_y. We renormalize this expression by substituting $K_1 \rightarrow 1$ and $K_3 \rightarrow K = K_3/K_1$:

$$I_p = I_x + KI_z$$
$$I_s = I_y + KI_z$$

Polarization anisotropy is defined as

$$r = \frac{I_{||} - I_{\perp}}{I_{||} + 2I_{\perp}}$$

For excitation light along the *x* axis, we associate

$$I_{||} = I_x$$
$$I_{\perp} = I_y = I_z$$

Using these expressions, we find that

$$I_p = I_{||} + KI_{\perp}$$
$$I_s = (1 + K)I_{\perp}$$

Further manipulation gives

$$I_{||} - I_{\perp} = I_p - I_s$$
$$I_{||} + 2I_{\perp} = I_p + \frac{2 - K}{1 + K}I_s$$

So, we calculate the polarization anisotropy as

$$r = \frac{I_p - I_s}{I_p + \frac{2 - K}{1 + K}I_s}$$

For nonzero *K*, the true *r* should be larger than what we measured. The deviation is less than 10% for $K = K_3/K_1 = 0.3$ (section III.B) and is negligible in comparison with the shot noise induced broadening of *r* distribution. Therefore, the conclusions we drew earlier from diffusing proteins are still valid even in the presence of the depolarization due to the objective.

IV. Conclusion

The polarization response of a single fluorophore, probed with the exquisite sensitivity of recently developed single-molecule spectroscopic techniques can yield detailed insights into rotational dynamics on the single-molecule level. Such insight cannot be obtained from conventional ensemble polarization studies. Under favorable circumstances, these novel single-molecule polarization techniques could lead to the identification of conformational states of biological macromolecules, both immobilized and freely diffusing in solution. The time evolution of a fluorophore's rotational dynamics can be measured with millisecond time resolution for surface immobilized molecules. Proper surface immobilization schemes that minimize the hindrance of the fluorophore's freedom of motion due to surface interactions should be sought. The polarization response of single fluorophores attached to biological macromolecules is already being used to probe their function, and with properly designed biological constructs it should be possible to observe single-molecule reactions in real time.

Acknowledgment. We thank Alice Y. Ting and Peter G. Schultz for the gift of protein samples. This work was supported by the Laboratory Directed Research and Development Program of Lawrence Berkeley National Laboratory under U.S. Department of Energy, Contract DE-AC03-76SF00098 and Office of Naval Research Contract N0001498F0402. T.A.L. is supported by a NSF Graduate Felloship.

References and Notes

(1) Shera, E. B.; Seitzinger, N. K.; Davis, L. M.; Keller, R. A.; Soper, S. A. *Chem. Phys. Lett.* **1990**, *174*, 553.
(2) Betzig, E.; Chichester, R. J. *Science* **1993**, *262*, 1422.
(3) Ambrose, W. P.; Goodwin, P. M.; Martin J. C. et al. *Phys. Rev. Lett.* **1994**, *72*, 160.
(4) Nie, S.; Chiu, D. T.; Zare, R. N. *Science* **1994**, *266*, 1018.
(5) Xie, X. S.; Dunn, R. C. *Science* **1994**, *265*, 361.
(6) Ambrose, W. P.; Goodwin, P. M.; Martin, J. C.; Keller, R. A. *Science* **1994**, *265*, 364.
(7) Trautman, J. K.; Macklin, J. J.; Brus, L. E.; Betzig, E. *Nature* **1994**, *369*, 40.
(8) Th. Schmidt et al. *J. Phys. Chem.* **1995**, *99*, 17662.
(9) Funatsu, T.; Harada, Y.; Tokunaga, M.; Saito, K.; Yanagida, T. *Nature* **1995**, *374*, 555.
(10) Macklin, J. J.; Trautman, J. K.; Harris, T. D.; Brus, L. E. *Science* **1996**, *272*, 255.
(11) Ha, T.; Enderle, Th.; Ogletree, D. F.; Chemla, D. S.; Selvin, P.; Weiss, S. *Proc. Natl. Acad. Sci. U.S.A.* **1996**, *93*, 624.
(12) Vale, R. D.; Funatsu, T.; Pierce, D. W.; Romberg, L.; Harada, Y.; Yanagida, T. *Nature* **1996**, *380*, 451.
(13) Ha, T.; Enderle, Th.; Chemla, D. S.; Selvin, P.; Weiss, S. *Phys. Rev. Lett.* **1996**, *77*, 3979.
(14) Lu, H. P.; Xie, X. S. *Nature* **1997**, *385*, 143.
(15) Dickson, R. M.; Norris, D. J.; Tzeng, Y. L.; Moerner, W. E. *Science* **1996**, *274*, 966.
(16) Dickson, R. M.; Cubitt, A. B.; Tsien, R. Y.; Moerner, W. E. *Nature* **1997**, *388*, 355.
(17) Xu, X. N.; Yeung, E. S. *Science* **1997**, *275*, 1106.
(18) Vanden Bout, D. A.; Yip, W. T.; Hu, D.; Fu, D. K.; Swager, T. M.; Barbara, P. F. *Science* **1997**, *277*, 1074.
(19) Ruiter, A. G. T.; Veerman, J. A.; Garcia-Parajo, M. F.; van Hulst, N. F. *J. Phys. Chem. A* **1997**, *101*, 7318.
(20) Sase, I.; Miyata, H.; Ishiwata, S.; Kinosita, K. *Proc. Natl. Acad. Sci. U.S.A.* **1997**, *94*, 5646.
(21) Bopp, M. A.; Jia, Y. W.; Li, L. Q.; Cogdell, R. J.; Hochstrasser, R. M. *Proc. Natl. Acad. Sci. U.S.A.* **1997**, *94*, 10630.
(22) Eggeling, C.; Fries, J. R.; Brand, L.; Gunther, R.; Seidel, C. A. M. *Proc. Natl. Acad. Sci. U.S.A.* **1998**, *95*, 1556. Schaffer, T.; Volkmer, A.; Eggeling, C.; Subramuniam, V.; Striker, G.; Seidel, C. A. M. *J. Phys. Chem. A* **1999**, *103*, 331.
(23) Ishijima, A.; Kojima, H.; Funatsu, T.; Tokunaga, M.; Higuchi, H.; Tanaka, H.; Yanagida, T. *Cell* **1998**, *92*, 161.
(24) Ha, T.; Glass, J.; Enderle, Th.; Chemla, D. S.; Weiss, S. *Phys. Rev. Lett.* **1998**, *80*, 2093.
(25) Warshaw, D. M.; Hayes, E.; Gaffney, D.; Lauzon, A. M.; Wu, J. R.; Kennedy, G.; Trybus, K.; Lowey, S.; Berger, C. *Proc. Natl. Acad. Sci. U.S.A.* **1998**, *95*, 8034.
(26) Yokota, H.; Saito, K.; Yanagida, T. *Phys. Rev. Lett.* **1998**, *80*, 4606.
(27) Ha, T.; Ting, A. Y.; Liang, J.; Caldwell, W. B.; Deniz, A. A.; Chemla, D. S.; Schultz, P. G.; Weiss, S. *Proc. Natl. Acad. Sci. U.S.A.* **1999**, *96*, 893.
(28) Ha, T.; Ting, A. Y.; Liang, J.; Deniz, A. A.; Chemla, D. S.; Schultz, P. G.; Weiss, S. *Chem. Phys.* To be published.
(29) Deniz, A. A.; Maxime Dahan, Ha, T.; Grunwell, J.; Faulhaber, A.; Chemla, D. S.; Weiss, S.; Schultz, P. G. *Proc. Natl. Acad. Sci. U.S.A.* **1999**, *96*, 3620.
(30) Dahan, M.; Deniz, A.; Ha, T.; Grunwel, J.; Chemla, D. S.; Schultz, P. G. Weiss, S. *Chem. Phys*. In press.
(31) Weiss, S. *Science* **1999**, *283*, 1676.
(32) For a review, see: Cantor, C. R.; Schimmel, P. R. Biophysical Chemistry W. H. Freeman and Co.: San Francisco, 1980.
(33) Güttler, F.; Sepiol, J.; Plakhotnik, T.; Mitterdorfer, A.; Renn, A.; Wild, U. P.; *J. Lumin*. **1993**, *56*, 29.
(34) Bethe, H. A. *Phys. Rev*. **1944**, *66*, 163.
(35) Trautman, J. K. Private communication.
(36) Sepiol, J.; Jasny, J.; Keller, J.; Wild, U. P. *Chem. Phys. Lett.* **1997**, *274*, 444.
(37) Dickson, R. M.; Norris, D. J.; Moerner, W. E. *Phys. Rev. Lett.* **1998**, *81*, 5322.
(38) Schütz, G. J.; Schindler, H.; Schmidt, Th. *Opt. Lett.* **1997**, *22*, 651.
(39) Ha, T.; Enderle, T.; Chemla, D. S.; Weiss, S. *IEEE J. Sel. Top. Quantum Electron.* **1996**, *2*, 1115.
(40) Ha, T.; Chemla, D. S.; Enderle, Th.; Weiss, S. *Appl. Phys. Lett*. **1997**, *70*, 782.
(41) Ha, T.; Chemla, D. S.; Enderle, Th.; Weiss, S. *Bioimaging* **1997**, *5*, 99.
(42) Wahl, P. *Chem. Phys.* **1975**, *7*, 210.
(43) Richards, B.; Wolf, E. *Proc. R. Soc. London A* **1959**, *253*, 358.
(44) Koshioka, M.; Sasaki, K.; Masuhara, H. *Appl. Spectrosc.* **1995**, *49*, 224.
(45) Kant, R. *J. Mod. Opt.* **1993**, *40*, 337.
(46) Axelrod, D. *Biophys. J.* **1979**, *26*, 557.
(47) Lukosz, W.; Kunz, R. E. *J. Opt. Soc. Am*. **1997**, *67*, 1607−1619.
(48) Lukosz, W. *J. Opt. Soc. Am*. **1979**, *69*, 1495.
(49) Hellen, E. H.; Axelrod, D. *J. Opt. Soc. Am. B* **1987**, *4*, 337−350.
(50) Ehrenberg, M.; Rigler, R. *Chem. Phys*. **1974**, *4*, 390.
(51) Aragon, S. R.; Pecora, R. *J. Chem. Phys.* **1976**, *64*, 1791.